

Article

Analyzing HDPE Thermal and Catalytic Degradation in Hydrogen Atmosphere: A Model-Free Approach to the Activation Energy

Cátia S. Costa ¹, A. Fernandes ¹, Marta Munoz ² , M. Rosário Ribeiro ^{1,*}  and João M. Silva ^{1,3} 

¹ Centro de Química Estrutural, Institute of Molecular Sciences, Departamento de Engenharia Química, Instituto Superior Técnico, Universidade de Lisboa, 1049-001 Lisboa, Portugal; catia.s.costa@tecnico.ulisboa.pt (C.S.C.); auguste.fernandes@tecnico.ulisboa.pt (A.F.); jmsilva@deq.isel.ipl.pt (J.M.S.)

² Departamento de Matemática Aplicada, Ciencia e Ingeniería de los Materiales y Tecnología Electrónica, Universidad Rey Juan Carlos, 28933 Madrid, Spain; marta.munoz@urjc.es

³ Departamento de Engenharia Química, Instituto Superior de Engenharia de Lisboa, Instituto Politécnico de Lisboa, 1959-007 Lisboa, Portugal

* Correspondence: rosario@tecnico.ulisboa.pt

Abstract: Despite the great interest in thermochemical processes for converting plastic waste into chemical feedstocks or fuels, their kinetics are still a less studied topic, especially under reductive conditions. In the present work, non-isothermal thermogravimetric analysis is used to study the thermal and catalytic conversion of HDPE promoted by parent and metal-based H-USY (15) and H-ZSM-5 (11.5) zeolites under a reducing hydrogen atmosphere. Additionally, the respective kinetic parameters (apparent activation energy, E_a , and frequency factor, A) were determined by applying two distinct model-free methods: Flynn–Wall–Ozawa (FWO) and Kissinger–Akahira–Sunose (KAS). The results showed that E_a of the thermal degradation of HDPE has an average value of 227 kJ/mol for both methods. In the presence of H-USY (15) and H-ZSM-5 (11.5) zeolites, E_a is strongly reduced and is highly dependent on conversion. In the case of H-USY (15), E_a varies from 78 to 157 kJ/mol for the KAS method and from 83 to 172 kJ/mol for the FWO method. Slightly lower values are reported for H-ZSM-5, with E_a values in the range of 53–122 kJ/mol for KAS and 61–107 kJ/mol for FWO. The presence and type of the metal source (Ni, Pt, or Pd) also affect the kinetic parameters of the reaction. The mean E_a values follow the order: Ni > Pt \approx Pd for H-USY (15) or H-ZSM-5 zeolites. Accordingly, both parent and metal-based H-USY (15) and H-ZSM-5 zeolites can significantly reduce energy consumption in HDPE hydrocracking, thus promoting a more sustainable conversion of plastic waste.

Keywords: kinetic parameters; model-free or iso-conversional methods; Kissinger–Akahira–Sunose; Flynn–Wall–Ozawa; HDPE conversion; zeolites



Citation: Costa, C.S.; Fernandes, A.; Munoz, M.; Ribeiro, M.R.; Silva, J.M. Analyzing HDPE Thermal and Catalytic Degradation in Hydrogen Atmosphere: A Model-Free Approach to the Activation Energy. *Catalysts* **2024**, *14*, 514. <https://doi.org/10.3390/catal14080514>

Academic Editor: Guido Busca

Received: 21 June 2024

Revised: 2 August 2024

Accepted: 3 August 2024

Published: 9 August 2024



Copyright: © 2024 by the authors. Licensee MDPI, Basel, Switzerland. This article is an open access article distributed under the terms and conditions of the Creative Commons Attribution (CC BY) license (<https://creativecommons.org/licenses/by/4.0/>).

1. Introduction

Over the past 50 years, plastics have provided and improved our lifestyle. However, changes in consumption and production patterns are leading to a rapid increase in plastic waste (PW) generation, which is becoming one of the most pressing environmental concerns [1]. The conversion of PW into resources is crucial for increasing efficiency and fostering circularity [2]. In recent years, chemical recycling and in particular, thermochemical processes, such as thermal and catalytic cracking, have emerged as promising options for converting PW into chemical feedstocks or fuels [3]. Thermal cracking (TC) is a widely used process but it suffers from two main problems: limited conversion of the feedstock at low temperatures and a wide carbon molecular weight distribution, leading to low selectivity for high-value products [4,5]. Catalytic cracking (CC), conversely, requires a catalyst [6]

and allows the process to be carried out at lower temperatures, improving the yield and selectivity of the desired products [7]. Several authors have studied the TC and CC of polymers under an inert atmosphere, in particular polyethylene (PE) and polypropylene (PP), over different acidic catalysts [8], obtaining *n*-paraffins and olefins as the main products. However, to develop more efficient processes for the thermal and catalytic conversion of plastics, knowledge of the reaction kinetics is extremely important [9,10]. The kinetic parameters, apparent activation energy (E_a) and frequency factor (A), are closely related to the reaction and are highly dependent on the feedstock used, the reaction mechanism, the degree of conversion, and the kinetic study method chosen [11]. Thermogravimetric analysis (TGA) is one of the most widely used techniques to study the mechanism and determine the kinetic parameters (A and E_a) of thermal and catalytic cracking of HDPE under different conditions.

The activation energy values found in the literature for the degradation of HDPE in the absence of catalysts, and in an inert atmosphere, typically range from 204 to 473 kJ/mol, with most values clustering around 230–270 kJ/mol [10,12–15]. The use of catalysts, such as H-Al-MCM-41 [16], H-USY [17,18], H-Y [17,19], and H-ZSM-5 [17–19], can significantly lower the activation energy, with values ranging from 60 to 185 kJ/mol, indicating a more facilitated degradation process.

In turn, the chemical conversion of plastics by CC under hydrogen (H_2) pressure—hydrocracking—offers many advantages when compared to alternative TC and CC routes. The ability to process a wide range of feedstocks, produce more stable and valuable products, and reduce the coke precursors responsible for deactivating the catalyst are the most significant [20,21]. However, to the best of our knowledge, there are no TGA kinetic studies for the conversion of HDPE conducted in a reducing atmosphere.

Therefore, the main objective of this work is to determine the apparent activation energy (E_a) for the thermal and the catalytic conversion of HDPE under H_2 over parent and metal-based H-USY (15) and H-ZSM-5 (11.5) zeolites. Two integral iso-conversional methods, based on the analysis of multiple TGA curves measured at different heating rates, were applied, namely, Flynn-Wall-Ozawa and Kissinger–Akahira–Sunose. The impact of incorporating a metal function (Ni, Pt, or Pd) to the parent zeolites on the apparent E_a , associated with the multistep processes occurring in HDPE hydrocracking is examined and discussed.

Therefore, the primary objective of this study is to ascertain the apparent activation energy (E_a) associated with the thermal and catalytic conversion of HDPE under a H_2 atmosphere. The catalytic systems under investigation include the H-USY (15) and H-ZSM-5 (11.5) zeolites. The impact of incorporating a metal function (Ni, Pt, or Pd) into the parent zeolites on the apparent E_a associated with the multistep process occurring in HDPE hydrocracking is examined and discussed. Two integral iso-conversional methods, based on the analysis of multiple TGA curves measured at different heating rates, were applied, namely, Flynn-Wall-Ozawa (FWO) and Kissinger–Akahira–Sunose (KAS)

2. Theoretical Approach

Several methods are used in the literature for non-isothermal solid state-kinetics calculations based on TGA data. These methods fall into two major categories: model-fitting and model-free or iso-conversional methods [22–24].

Model-fitting methods are applied to determine E_a and A from a single simulated curve [25]. In this case, TGA data are fitted to different reaction models (Table S1 of the Supporting Information) in order to obtain the best statistical fit and consequently the most suitable kinetic parameters (E_a and A). The main advantage of model-fitting methods, when applied to solid-state reactions, is their experimental simplicity, since only a single TGA experiment is required to determine the kinetic data. However, model-fitting methods also present several problems, the most important of which is the inability to unequivocally identify the unknown reaction model [26].

Conversely, model-free or iso-conversional methods allow the determination of the Arrhenius parameters without pre-selecting a reaction model and a reaction order. However, from an experimental point of view, this approach is much more time-consuming as it requires TGA curves at different heating rates to obtain a dependence of the kinetic parameters on conversion and/or temperature [27]. According to the International Confederation for Thermal Analysis and Calorimetry (ICTAC) Kinetics Committee [28], the use of multi-rate programs is recommended for the calculation of reliable kinetic parameters. This methodology not only avoids the risk of obtaining erroneous kinetics, due to an inappropriate reaction model but also allows the prediction of some mechanistic steps, since E_a can be estimated for a range of conversion values [29,30]. Several authors have contributed to the extension and consolidation of the knowledge in IC methods, such as Friedman [31], Flynn and Wall [32,33], Ozawa [34], Kissinger [35], and Vyazovkin [28,36], among others.

According to the authors listed above, the rate of a chemical reaction, in this specific case, the rate of HDPE degradation, can be described as follows:

$$\frac{dx}{dt} = K(T)f(x) \quad (1)$$

where $K(T)$ is the kinetic constant rate and $f(x)$ is a function depending on the reaction mechanism involved. The term x is defined as the advancement of the reaction and is expressed in terms of conversion according to the following equation:

$$x = \frac{x_0 - x_t}{x_0 - x_f} \quad (2)$$

where x_0 and x_f are the initial and final solid mass, respectively; and x_t the mass at a specific time t . In its turn, the temperature-dependent term, $K(T)$ is generally denoted as:

$$K(T) = A \exp\left(-\frac{E_a}{RT}\right) \quad (3)$$

where A is the frequency factor (min^{-1}), E_a is the apparent Activation Energy (J/mol), R is the gas constant (8.314 J/K mol), and T is the absolute temperature. The generalized kinetic rate equation is expressed in terms of x and obtained by the combination of the three previous equations:

$$\frac{dx}{dt} = K(T)f(x) = A \exp\left(-\frac{E_a}{RT}\right)f(x) \quad (4)$$

For a dynamic TGA process, the heating rate can be defined as $\beta = dT/dt$. Including β in the previous equation results in the following relationship:

$$\frac{dx}{dt} = \frac{1}{\beta} A \exp\left(-\frac{E_a}{RT}\right)f(x) \quad (5)$$

Therefore, the integral form of the inverse of $f(x)$, which describes the reaction kinetic model, can be expressed as follows:

$$G(x) = \int_0^x \frac{dx}{f(x)} = \frac{A}{\beta} \int_{T_0}^T \exp\left(-\frac{E_a}{RT}\right) dT = \frac{AE_a}{\beta R} p(u) \quad (6)$$

the term $p(u)$ represents a temperature-dependent integral, without an analytical solution

$$p(u) = \int_0^u \exp\left(\frac{-u}{u^2}\right) du \quad (7)$$

with

$$u = \frac{E_a}{RT} \quad (8)$$

However, Equation (6) can be solved by using different approximations for the $p(u)$ function. Accordingly, several integral model-free iso-conversional methods have been developed for the estimation of the kinetic parameters (E_a and A).

For these methods, $p(u)$ can be expressed by the following general approximate equation:

$$p(u) = \frac{e^{(-C u - D)}}{u^B} \quad (9)$$

where the values of B , C , and D depend on the method applied.

By replacing Equation (9) in Equation (6), linearizing and simplifying, it is possible to obtain a general expression that relates $\ln(\beta_i/T_{x,i}^B)$ with $1/T_{x,i}$:

$$\ln\left(\frac{\beta_i}{T_{x,i}^B}\right) = \left\{ \ln\left[\frac{A}{G(x)}\right] - D + (1 - B) \ln\left(\frac{E_a}{R}\right) \right\} - C\left(\frac{E_a}{RT_{x,i}}\right) \quad (10)$$

This means that, at any constant conversion, a linear relationship is obtained by plotting $\ln(\beta_i/T_{x,i}^B)$ against $1/T_{x,i}$. Consequently, from the slope of the line $[-CE_a/R]$, it is possible to calculate the E_a value for the corresponding extent of conversion, while from the line interception $[\ln[A/G(x)] - D + (1 - B) \ln(E_a/R)]$, a combination of the pre-exponential factor with $G(x)$, $[\ln A/G(x)]$ [37] is obtained.

In this study, the Flynn–Wall–Ozawa (FWO) and Kissinger–Akahira–Sunose (KAS) methods were employed to ascertain E_a . In accordance with the FWO method [32], which employs Doyle’s approximation [38], the values of B , C , and D are 0, 1.0516, and 5.3305, respectively. In the case of the KAS method, which employs the more accurate approximation of Murray and White [39], the values of B , C , and D are 2, 1, and 0, respectively. Substituting B , C , and D by the respective values into Equation (10), yields the final expressions for each method, as outlined in Table 1.

Table 1. Model-free methods applied in this study.

Method	Expression	Plot
Flynn–Wall–Ozawa (FWO)	$\ln(\beta) = \ln\left(\frac{AE_a}{RG(x)}\right) - 5.311 - \frac{1.052E_a}{RT}$	$\ln(\beta)$ vs. $1/T$
Kissinger–Akahira–Sunose (KAS)	$\ln\left(\frac{\beta}{T^2}\right) = \ln\left(\frac{AR}{E_a G(x)}\right) - \frac{E_a}{RT}$	$\ln\left(\frac{\beta}{T^2}\right)$ vs. $1/T$

It is important to note that the accuracy of integral iso-conversional methods is constrained by the underlying assumptions upon which they are based. Alternative differential iso-conversional methods, such as the Friedman (FR) method, have been developed to address these limitations. However, the application of the FR method necessitates numerical differentiation of typically noisy TGA data, which can give rise to other issues, including numerical instabilities and discontinuous E_a profiles.

3. Results

3.1. Catalyst Characterization

The PXRD diffractograms of the parent and metal-based H-USY (15) and H-ZSM-5 (11.5) zeolites are displayed in Figures S1 and S2 of the Supporting Information. For the H-USY zeolite, peaks at $2\theta = 6.2, 10.3, 12.1, 15.9, 18.9, 20.7, 24.0,$ and 27.5° are observed. Such peaks are characteristic of the FAU framework in USY zeolites [40]. In contrast, for H-ZSM-5 (11.5), diffraction peaks are observed at $2\theta = 7.9, 8.8, 14\text{--}17,$ and $23\text{--}25^\circ$, which are characteristic of the MFI framework in ZSM-5 zeolites [41]. After incorporation of Ni, Pt, and Pd no signs of structural changes are observed, as the metal-based zeolites show the characteristic peaks of the parent structure. However, in the case of Ni-based H-USY (15) and H-ZSM-5 (11.5) new diffraction peaks are observed at $2\theta = 7.9$ and 8.8 , typical of Ni^0 species. Pt^0 and Pd^0 reflection peaks are not observed in the PXRD diffractograms as the metal content (0.5 wt.%) is below the detection limit of the instrument. A slight decrease

($\leq 10\%$) [Table 2] in the crystallinity of the parent systems is detected for all the metal-based systems, as a result of metal incorporation.

Table 2. Physical and chemical properties of parent and metal-based H-USY (15) and H-ZSM-5 (11.5) zeolites.

Catalyst	Crystallinity (%)	S_{ext} (m ² /g)	V_{micro} (cm ³ /g)	V_{meso} (cm ³ /g)	V_{total} (cm ³ /g)	Weak Acidity (μmol/g)	Strong Acidity (μmol/g)	Total Acidity (μmol/g)
H-USY (15)	100	189	0.25	0.23	0.48	332	319	651
Ni (5)/H-USY (15)	97.4	170	0.24	0.24	0.48	288	245	533
Pt (0.5)/H-USY (15)	93.7	184	0.24	0.24	0.48	364	256	620
Pd (0.5)/H-USY (15)	93.7	180	0.24	0.23	0.47	324	301	625
HZSM-5 (11.5)	100	114	0.13	0.10	0.23	740	530	1270
Ni (5)/H-ZSM-5 (11.5)	91.2	78	0.12	0.07	0.19	670	500	1170
Pt (0.5)/H-ZSM-5 (11.5)	95.7	61	0.10	0.05	0.15	650	530	1180
Pd (0.5)/H-ZSM-5 (11.5)	97.6	77	0.10	0.06	0.17	650	500	1150

In terms of textural properties, the H-USY (15) zeolite exhibits a higher external surface area (S_{ext}) and a higher microporous volume (V_{micro}), due to its small crystal sizes (0.7 μm) and its microporous structure with a secondary mesoporosity, respectively. According to the literature [42], H-USY-type zeolites have a three-dimensional pore structure in which the basic sodalite structural units are assembled in spherical supercages with a diameter of 1.3 nm and an aperture window of 0.7 nm. Conversely, the HZSM-5 zeolite is composed of a three-dimensional structure interconnected by two channels with 10-membered rings with the following dimensions: 0.51 × 0.55 nm (sinusoidal channels) and 0.56 × 0.53 nm (straight channels) [43]. Upon metal incorporation a slight reduction in S_{ext} and V_{micro} is observed, especially for H-ZSM-5 (11.5) zeolites, indicating the deposition of Ni, Pt, and Pd particles on the external surface of the zeolite and/or inside its porous structure. Nevertheless, H-ZSM-5 (11.5) reveals a higher number of total acid sites, 1270 μmol/g, than H-USY (15) zeolite, 651 μmol/g. However, in both systems, the addition of a metallic source leads to a slight decrease in total acidity, probably due to the partial blockage of the pores opening by the metallic particles, which limits the access of the NH₃ to the active sites. This fact is corroborated by N₂ sorption results.

3.2. Thermogravimetric Analysis

In order to evaluate the decomposition of HDPE in the presence and absence of H-ZSM-5 (11.5) and H-USY (15) zeolites, the TGA profiles at a constant heating rate (10 °C/min) are displayed in Figure 1a, while the temperatures at which HDPE mass loss is 5, 50, and 95% ($T_{5\%}$, $T_{50\%}$, and $T_{95\%}$) are shown in Figure 1b.

According to the data, the HDPE thermal degradation occurs in one single step, starting at 433 °C and ending at 488 °C. Similar HDPE degradation profiles are reported in the literature under inert conditions, as well as identical degradation ranges (between 381 and 501 °C) [44–46]. Instead, the catalyst seems to play a crucial role in the degradation. In this case, a substantial decrease in the energy requirements is observed upon the addition of H-USY (15) and H-ZSM-5 (11.5). Although both catalysts reduce HDPE degradation temperatures, H-USY (15) is the one that allows a higher diminishment, around 162 °C on $T_{5\%}$. For the same mass loss, the H-ZSM-5 (11.5) allows for a reduction of 115 °C. According to the literature [47,48], the catalytic activity of zeolites in this type of reaction is strongly dependent on the acidity and the accessibility of the acid sites of the catalyst. Although the H-USY (15) zeolite exhibits a lower acid content compared to H-ZSM-5 (11.5), it has a three-dimensional channel system with large cavities, also known as supercages. These supercages, together with a higher external surface area, reduce the diffusional limitation constraints, and favor the access of polymer macromolecules to the active sites. These facts lead to an increase in cracking reactions and consequently to an easy degradation of HDPE [8].

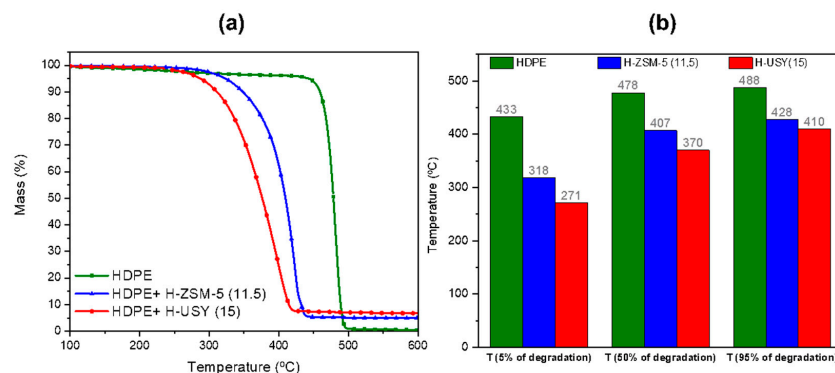


Figure 1. TGA profiles (a) and temperature at which mass loss is 5, 50, and 95% ($T_{5\%}$, $T_{50\%}$, and $T_{95\%}$) (b), in presence and absence of H-USY (15) and H-ZSM-5 (11.5) zeolites.

Together with the physical and chemical features, the heating rate (β) used in the TGA experiments also has an important influence on HDPE degradation. The effect of β (5, 10, 15, and 20 °C/min) on the HDPE TGA profiles and first-order derivative (DTG) curves for the thermal and catalytic systems is displayed in Figure 2.

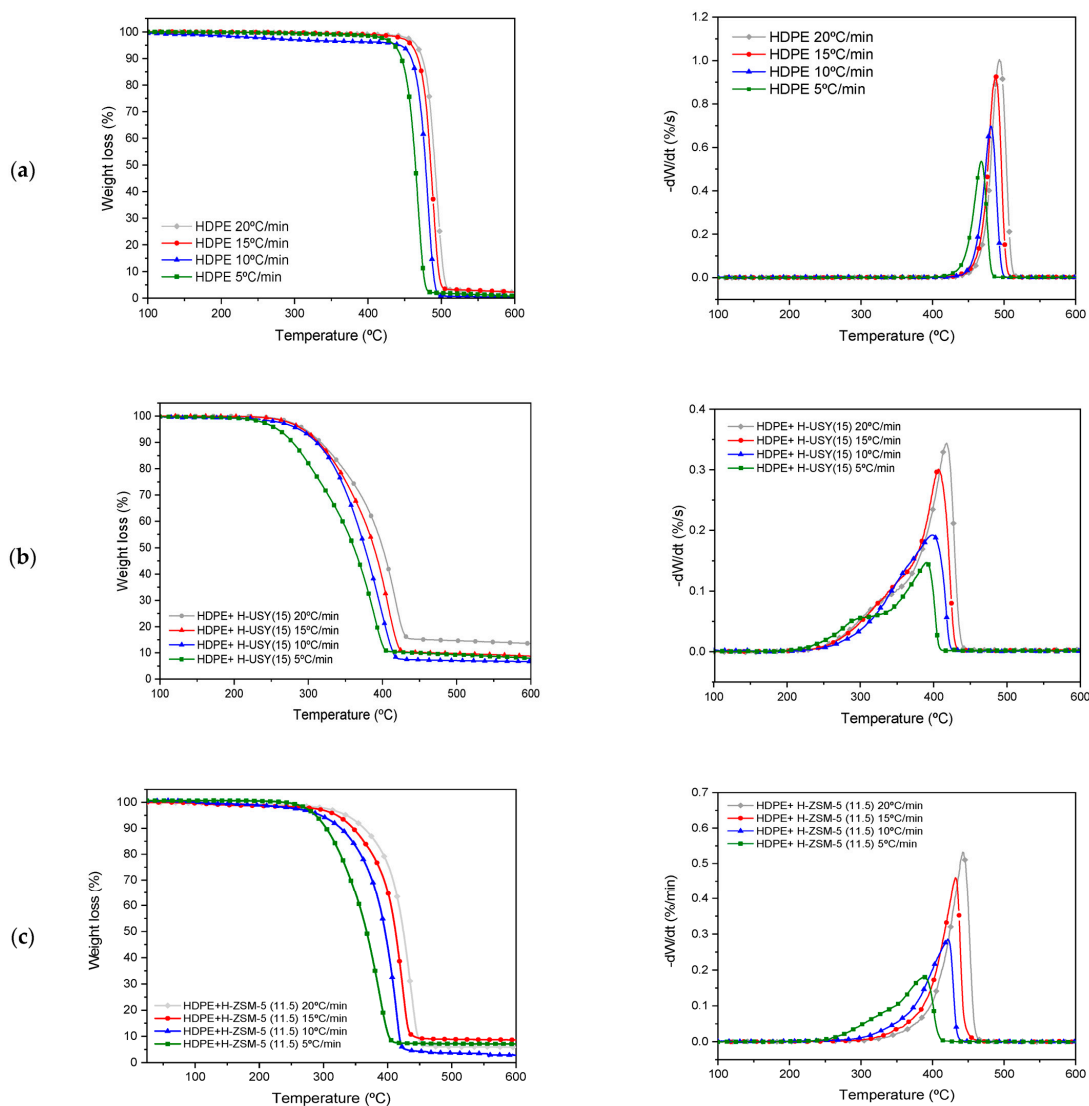


Figure 2. TGA and DTG profiles for thermal and catalytic degradation of HDPE under a H_2 atmosphere without catalyst (a) and over H-USY (15) (b) and H-ZSM-5 (11.5) (c).

The $T_{5\%}$, $T_{50\%}$, and $T_{95\%}$ and the maximum weight loss temperature (T_m), obtained from the peak of the DTG curve, are summarized in Table 3.

Table 3. Temperature at which mass loss is 5, 50, and 95% ($T_{5\%}$, $T_{50\%}$, and $T_{95\%}$) calculated from the TGA curves and maximum degradation temperature (T_m) determined from DTG profiles.

Sample	β ($^{\circ}\text{C}/\text{min}$)	Temperature ($^{\circ}\text{C}$)			
		$T_{5\%}$	$T_{50\%}$	$T_{95\%}$	T_m
HDPE	5	433	463	473	468
	10	433	478	488	480
	15	455	484	494	488
	20	463	489	501	493
HDPE + H-USY (15)	5	255	354	398	392
	10	271	370	410	399
	15	289	382	418	408
	20	292	394	431	418
HDPE + H-ZSM-5 (11.5)	5	283	362	397	389
	10	318	407	428	421
	15	325	413	430	432
	20	329	421	443	442

Data reveal that in the absence of a catalyst, an increase in β delays the degradation rate of HDPE, leading to a shift of $T_{5\%}$, $T_{50\%}$, and $T_{95\%}$ to higher temperatures. For the extreme cases of β (5 and 20 $^{\circ}\text{C}/\text{min}$), the HDPE degradation range varies from 433 to 473 $^{\circ}\text{C}$ and from 463 to 501 $^{\circ}\text{C}$, respectively. The DTG results also show that the maximum loss rate occurs at 468 $^{\circ}\text{C}$ ($\beta = 5$ $^{\circ}\text{C}/\text{min}$) and 493 $^{\circ}\text{C}$ ($\beta = 20$ $^{\circ}\text{C}/\text{min}$), indicating heat and mass transfer limitations during the thermal run for higher heating rates [49,50].

A shift in the mass loss curve to a higher temperature as the heating rate increased was also observed when both catalysts were used. In the case of H-USY (15), the degradation temperature range suffers a significant increase with β , varying from 255–398 $^{\circ}\text{C}$ at 5 $^{\circ}\text{C}/\text{min}$ to 292–431 $^{\circ}\text{C}$ at 20 $^{\circ}\text{C}/\text{min}$. For H-ZSM-5 (11.5), a change of the same order is observed. For both catalytic systems, although the TGA profiles present an identical shape for different β values, the DTG data reveal the appearance of an additional peak at lower heating rates. In previous studies, the authors concluded that at sufficiently low decomposition rates, overlapping adjacent peaks can be separated due to lower heat transfer limitations. In this case, the different decomposition reactions that occur simultaneously at higher β can be identified separately at lower β [51].

3.3. Thermal and Catalytic Cracking Kinetics

Kinetic analysis plays a main role in reactor design and scale-up processes, providing insight into the reaction mechanism [52]. The objective of kinetic analysis is the interpretation of the experimentally determined kinetic parameters (E_a and A), each of which is associated with a fundamental theoretical concept. E_a represents the minimum amount of energy required for a reaction to occur and is strongly dependent on the nature and concentration of the reactants, the reaction conditions, and the presence or absence of a catalyst and its type [53]. In contrast, A is related to the frequency of vibrations of the activated complex.

3.3.1. Apparent Activation Energy (E_a)

The E_a values for both the thermal and catalytic degradations of HDPE under a reducing atmosphere were calculated by applying the FWO, and KAS methods to the previous TGA data at different β values.

Figure 3 depicts the fitting results obtained from the model-free methods plots for the thermal degradation of HDPE. The resulting E_a and A values and correlation coefficient data are listed in Table 4 for thermal and catalytic conditions.

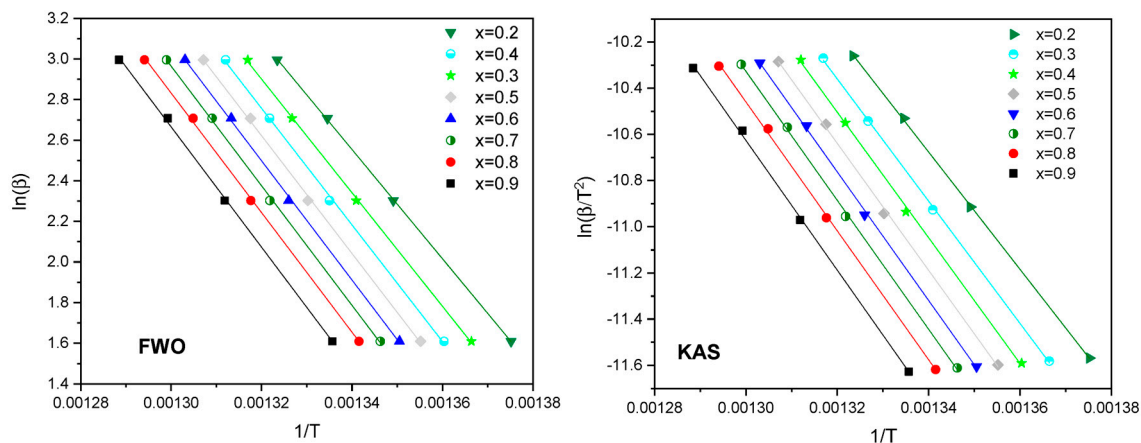


Figure 3. Linear fitting curves under distinct conversion levels for model-free methods applied to the HDPE thermal degradation TGA data.

Table 4. E_a , $\ln(A/G(x))$, and R^2 in function of the extent of conversion (x) determined by distinct model-free methods.

	x	FWO			KAS		
		E_a (kJ/mol)	$\ln(A/G(x))$	R^2	E_a (kJ/mol)	$\ln(A/G(x))$	R^2
HDPE	0.2	212.5	33.8	1.000	211.2	33.5	1.000
	0.3	220.9	34.9	1.000	220.0	34.8	1.000
	0.4	226.9	35.8	0.999	226.2	35.6	0.999
	0.5	229.2	36.0	0.999	228.6	35.9	0.999
	0.6	232.0	36.3	0.999	231.5	36.2	0.999
	0.7	232.7	36.3	0.999	232.3	36.2	0.999
	0.8	233.0	36.2	0.999	233.0	36.1	0.999
	0.9	234.1	36.3	0.999	233.7	36.1	0.999
	Av.	227.7	35.7	0.999	227.1	35.6	0.999
HDPE+ H-USY (15)	0.2	83.8	16.1	0.919	78.3	14.4	0.899
	0.3	93.1	17.4	0.976	87.7	15.8	0.971
	0.4	104.7	19.1	0.998	99.5	17.6	0.997
	0.5	115.0	20.5	0.988	110.2	19.3	0.985
	0.6	126.0	22.2	0.979	121.6	21.1	0.975
	0.7	137.0	23.9	0.970	133.0	22.9	0.965
	0.8	148.8	25.7	0.967	145.3	24.9	0.961
	0.9	172.2	29.6	0.988	157.5	23.8	0.810
	Av.	122.6	21.8	0.973	116.6	20.0	0.946
HDPE+ H-ZSM-5 (11.5)	0.2	60.6	10.9	0.889	53.3	7.8	0.849
	0.3	63.5	11.1	0.900	56.1	8.6	0.865
	0.4	69.5	11.9	0.904	62.2	9.6	0.873
	0.5	76.6	13.0	0.909	69.6	10.8	0.882
	0.6	84.3	14.2	0.915	77.5	12.2	0.892
	0.7	91.2	15.3	0.918	84.7	13.4	0.897
	0.8	98.5	16.4	0.926	92.2	14.7	0.908
	0.9	106.9	17.7	0.929	122.2	17.1	0.994
	Av.	81.4	13.8	0.911	77.2	11.8	0.895

Regarding the thermal data, correlation coefficients (R^2) higher than 0.999 are observed, indicating an excellent fit of the method to the experimental data and an accurate estimation of E_a . Moreover, it is observed that the fitted lines are approximately parallel, suggesting a unification of multiple reactions mechanism [29,54]. In this case, the E_a varies between approximately 211 and 234 kJ/mol for both the FWO and KAS methods as the HDPE conversion increases. The mean E_a value for all methods is 227 kJ/mol.

To the best of our knowledge, this is the first study reported in the literature to employ non-isothermal methods to determine the E_a for the thermal and catalytic degradation of HDPE in a reductive H_2 atmosphere. It should be noted that the present results fall within the range reported by other authors for the E_a of the thermal degradation of HDPE in an inert atmosphere (203–250 kJ/mol) [10,12,13,15,55].

When a catalyst is added to the reaction, the linear correlation coefficients are lower than those obtained under thermal conditions ($0.895 \leq R^2 \leq 0.973$), indicating a less accurate estimation. This could be due to: (i) slight differences in the amount of the catalyst used to perform the TGA experiments (~2–5%), which could affect the TGA profiles; or, (ii) poorer model fit for more complex mechanisms. As expected, the presence of H-USY (15) and H-ZSM-5 (11.5) zeolites leads to a significant reduction in E_a , since the reaction rate increases. With regard to the H-USY (15) data, it can be observed that the E_a values vary with the extent of the reaction. The values range from 78 to 157 kJ/mol for the KAS methods and from 83 to 172 kJ/mol for the FWO method. In the case of the H-ZSM-5 (11.5) zeolite, the E_a values vary between 53 and 122 kJ/mol for the KAS method and between 60 and 107 kJ/mol for the FWO method. The differences between the ranges of E_a for these two methods are more obvious for this catalyst, probably due to the worst linear fitting obtained for the iso-conversion plots (Table 4). The average E_a values are, however, quite similar, at 77 kJ/mol and 81 kJ/mol, respectively.

It is also interesting to note that the E_a observed for the catalytic conversion of HDPE over H-ZSM-5 (11.5) zeolite is significantly lower than over H-USY (15). Although H-USY (15) exhibits more suitable structural and textural properties for the reaction, H-ZSM5 zeolite has a higher number of acid sites, which are the main responsible for the HDC reactions [18]. The E_a values obtained are in agreement with those reported in the literature for both systems [H-USY (15): 95–118 kJ/mol and H-ZSM-5 (11.5): 60–124 kJ/mol] under an inert atmosphere [17–19].

In addition, data show that an E_a dependency with the extent of reaction is observed either for thermal or catalytic processes, suggesting that in all cases, multi-step complex mechanisms are involved [11,23], as previously observed. Similar behavior was observed by other authors [9,56,57], who reported an increase in the effective E_a with the course of the reaction for PE, as a result of the change in the limiting step during the reaction. For the particular case of thermal run, it is well known that the degradation occurs via a random scission mechanism followed by a radical transfer process [46,58]. Nevertheless, according to Peterson et al. [56] and Vyazovkin et al. [57], the lower E_a value observed in the early stages of the process is most likely related to the ignition of the degradation process, occurring at thermally labile bonds such as chain branches, unsaturated compounds, peroxides, and carbonyl groups, formed during the manufacture, storage, and processing of HDPE. Once the weak links are consumed, the limiting step of the degradation shifts towards the degradation initiated by random scission, leading to an increase in E_a . Instead, and although the E_a also increases with the extent of conversion, a distinct trend is observed for the catalytic systems, suggesting that a different mechanism is involved. This is corroborated by literature data, indicating that in the presence of a catalyst, HDPE degradation proceeds by the carbocation mechanism [59].

3.3.2. Effect of Adding a Metallic Source (Ni, Pt, Pd) to H-USY (15) and H-ZSM-5 (11.5) on the Kinetic Parameters

The catalytic conversion under a reducing atmosphere can proceed by distinct pathways depending on the catalyst used. In the presence of a monofunctional acidic catalyst, such as H-ZSM-5 (11.5) and H-USY (15), the reaction takes place by the carbocation mechanism, as mentioned before. However, when a metallic function is introduced on a monofunctional zeolite, the reaction mechanism changes. In this case, the metal favors dehydrogenation and hydrogenation reactions, while the remaining acidic centers are responsible for the cracking and isomerization reactions [60]. To evaluate the effect of the addition of a metal source on the catalytic degradation of HDPE in a H_2 atmosphere, Ni,

Pt, and Pd were added to H-USY (15) and H-ZSM-5 (11.5) zeolites. The TGA profiles are shown in Figure S3 of the Supporting Information.

Data show a positive effect on the degradation temperatures with the addition of Ni, Pt, and Pd either to H-USY (15) or to H-ZSM-5 (11.5), suggesting that the metallic function enhances the catalytic conversion of HDPE in the presence of a reducing H₂ atmosphere. This is due to the formation of olefinic intermediates on the metallic sites, which are easily converted into carbocation intermediates, contributing to an increase in the cracking rate. During the catalytic conversion over a monofunctional catalyst, these olefinic intermediates are not formed, thus reducing the rate of carbocation formation. However, the reduction in HDPE degradation temperatures is more pronounced for the noble metal than for the transition metal catalysts, leading to lower degradation temperatures according to the following order: Pd < Pt < Ni. The promising results obtained with noble metal systems are probably due to two main facts: (i) higher hydrogenation ability, which promotes the dehydrogenation/hydrogenation reactions [61]; and (ii) smaller particle size and consequently, higher dispersion of the metal on the H-USY (15) and H-ZSM-5 (11.5) supports (Figure S4 and Table S1 of the Supporting Information). However, from an economic point of view, the use of a Ni metallic source could be more favorable.

In order to understand how the presence of a metal source and its nature affects the kinetic parameters of the process, the KAS method was applied to TGA data at different heating rates ($\beta = 5, 10, 15,$ and 20 °C/min) using Ni-, Pt-, and Pd-based zeolites as catalysts. The HDPE degradation profiles at different β values are shown in Figure S3, while the resulting E_a and A values are summarized in Table 5.

Table 5. E_a , $\ln(A/G(x))$, and R^2 as a function of the conversion (x) determined by the KAS method for metal (Ni, Pt, and Pd)-based H-USY (15) and H-ZSM-5 (11.5) zeolites. * [Av-Average].

x	Ni/H-USY (15)		Pt/H-USY (15)		Pd/H-USY (15)	
	E_a (kJ/mol)	$\ln(A/G(x))$	E_a (kJ/mol)	$\ln(A/G(x))$	E_a (kJ/mol)	$\ln(A/G(x))$
0.2	153.4	30.4	219.3	45.1	202.2	43.8
0.3	149.7	28.8	182.5	36.1	180.4	35.4
0.4	141.3	26.6	165.3	31.8	161.2	32.3
0.5	134.3	24.8	153.4	28.9	149.7	29.2
0.6	131.4	23.9	144.0	26.6	144.5	28.5
0.7	132.9	23.9	136.6	24.7	132.2	26.7
0.8	137.7	24.5	131.5	23.4	123.5	25.3
0.9	159.6	28.2	130.0	22.7	127.6	24.5
Av.*	142.5	26.4	157.8	29.9	152.6	30.7
x	Ni/H-ZSM-5 (11.5)		Pt/H-ZSM-5 (11.5)		Pd/H-ZSM-5 (11.5)	
	E_a (kJ/mol)	$\ln(A/G(x))$	E_a (kJ/mol)	$\ln(A/G(x))$	E_a (kJ/mol)	$\ln(A/G(x))$
0.2	92.2	17.8	70.4	12.0	68.3	15.3
0.3	95.3	18.1	72.2	12.0	70.1	16.1
0.4	101.9	19.0	77.8	12.8	73.4	16.1
0.5	109.2	20.2	85.4	14.0	77.2	15.1
0.6	117.8	21.6	93.1	15.2	83.2	15.4
0.7	126.6	23.0	99.9	16.3	87.2	16.1
0.8	133.4	24.1	107.5	17.5	90.5	17.1
0.9	147.3	26.4	115.3	18.8	98.2	18.7
Av.*	115.5	21.3	90.2	14.8	87.0	16.2

As previously observed for parent zeolites, an increase in β leads to a shift in the degradation profiles of all the metal-based zeolites to higher temperatures, as a result of the reduced heat transfer and shorter exposure time of HDPE at a given temperature. Furthermore, higher heating rates also change kinetics, resulting in a slower degradation of HDPE macromolecules [24]. Data available in Table 5 also show that in the presence

of bifunctional catalysts, lower E_a values are observed compared to the thermal run data, as previously observed for the monofunctional systems. In general, a slight increase in the average E_a value is observed for the metal-based catalysts compared to the respective parent zeolites. This is probably the result of two main aspects, namely, (i) the contribution of the dehydrogenation/hydrogenation reactions promoted by metal source to the mean E_a , and (ii) the reduction of the total acidity of H-USY (15) and H-ZSM-5 (11.5) zeolites upon the impregnation process, both of which are essential to the cracking and isomerization steps [60].

Another explanation was suggested by the studies of Ramdoss and Tarrer [62], who developed a kinetic model combining series and parallel reactions for the conversion of post-consumer plastics to light oil, heavy oil, gas, and coke, in a H_2 atmosphere. Looking at the activation energies obtained for the various reaction pathways, it was found that the highest E_a values, 121.7 kJ/mol and 113.5 kJ/mol, correspond to the conversion of light and heavy liquids into gaseous fractions, respectively, while the lowest E_a value (11.8 kJ/mol) results from the conversion of heavier hydrocarbons into liquid fractions. Recent studies performed by our team show that there is a greater tendency to produce gaseous products over Ni-, Pt-, and Pd-based zeolites compared to their respective parent zeolites, which could thus contribute to the increase in E_a over the bifunctional catalysts. Miskolczi et al. [63], who calculated the E_a for the thermal and catalytic degradation of end-of-life vehicle plastic waste under a N_2 atmosphere, over H-Y and H-ZSM-5 (11.5) loaded with distinct metals (Fe, Sn, Ce, Mg, Ni, Cu, and Zn), also found that the addition of a metal source to the parent zeolites results in an increase in the apparent E_a of the reaction for all cases, in the order $Cu < Ce < Mg < Ni < Fe(III) < Fe(II) < Zn < Sn$, thus, corroborating our data.

4. Materials and Methods

4.1. Materials

Commercial high-density polyethylene (HDPE, MW = 155,000 g/mol; MWD = 5.4; $d = 0.95 \text{ g/cm}^3$ and $T_m = 140 \text{ }^\circ\text{C}$), was supplied by Repsol (Sines, Portugal) without additives and used in powder form.

The zeolite catalysts, NH_4 -ZSM-5(11.5) (CBV-2314) and H-USY (15) (CBV-720), were supplied by Zeolyst (Conshohocken, PA, USA). The metal salts, nickel nitrate hexahydrate ($Ni(NO_3)_2 \cdot 6H_2O$), and tetraamine platinum (II) nitrate ($Pt(NH_3)_4 \cdot (NO_3)_2$), used for the preparation of Ni- and Pt-impregnated catalysts were supplied by Merck (Darmstadt, Germany), both with a purity of 99%. The palladium nitrate ($Pd(NO_3)_2$) solution used for the preparation of Pd-impregnated zeolites was supplied by Sigma-Aldrich (St. Louis, MO, USA).

4.2. Catalyst Preparation

NH_4 -ZSM-5 was calcined at $500 \text{ }^\circ\text{C}$ for 6 h under an airflow of $4 \text{ L}\cdot\text{h}^{-1}\cdot\text{g}^{-1}$ in order to transform the ammonium form to the protonic form (H-ZSM-5 (11.5)). A plateau at $200 \text{ }^\circ\text{C}$, for 1 h, was carried out to remove the water and prevent the zeolite from steaming. A heating rate of $2 \text{ }^\circ\text{C}\cdot\text{min}^{-1}$ was used.

The preparation of Ni-, Pt-, and Pd-based zeolites was performed by the incipient wetness impregnation method, using an aqueous solution of $Ni(NO_3)_2 \cdot 6H_2O$, $Pt(NH_3)_4 \cdot (NO_3)_2$ and $Pd(NO_3)_2$, respectively. The volume of the metal precursor solution used was calculated to match the volume of the zeolite pores and was added dropwise to the support. The impregnated samples were air-dried at $80 \text{ }^\circ\text{C}$ for 24 h and then calcined at $500 \text{ }^\circ\text{C}$ in an airflow of $\text{L}\cdot\text{h}^{-1}\cdot\text{g}^{-1}$. Prior to use, all impregnated catalysts were also pre-activated in a reactor with an H_2 flow of $4 \text{ L}\cdot\text{h}^{-1}\cdot\text{g}^{-1}$ for 2 h, at $500 \text{ }^\circ\text{C}$ for Ni catalysts and at $450 \text{ }^\circ\text{C}$ for Pt and Pd catalysts.

4.3. Catalyst Characterization

The textural properties of the parent and metal-based catalysts were assessed by N₂ sorption. Measurements were performed at −196 °C using an Autosorb IQ apparatus from Quantachrome (Boynton Beach, FL, USA). Prior to measurement, the materials were degassed under vacuum at 90 °C for 1 h and then heated at 350 °C for 5 h. The external surface area (S_{ext}) and micropore volume (V_{micro}) were calculated using the t-plot method, while the total pore volume was determined from the adsorbed volume of nitrogen at a relative pressure (P/P_0) of 0.95. The difference between V_{total} and V_{micro} gives the mesopore volume (V_{meso}).

Powder X-ray diffraction (PXRD) analysis was used to obtain information on the phases present in the prepared catalysts, as well as to identify any damage to the zeolite materials upon metal incorporation. The PXRD experiments were carried out using a Bruker AXS Advance D8 diffractometer (Billerica, MA, USA) equipped with a 1D detector (SSD 160) and using a Ni filter, with a CuK α radiation source ($\lambda = 1.5406$ nm) and operating at 40 kV and 30 mA. The scanning range was from 5° to 80° (2 theta), with a step size of 0.03° and a step time of 2 s.

The density and strength distribution of acid sites of the zeolites were determined by ammonia temperature-programmed desorption (NH₃-TPD). In these experiments, the sample was pre-treated under helium atmosphere at 350 °C for 1 h and then cooled to 125 °C and ammonia-saturated in a stream of 15% NH₃/He at a flow of 30 mL/min, for 1 h. Prior to the desorption step, the sample was outgassed under helium at 125 °C for 30 min, to remove the physisorbed ammonia. Chemisorbed NH₃ was desorbed at a heating rate of 10 °C/min until 700 °C and the amount of ammonia desorbed in the effluent stream was detected by a thermal conductivity detector (TCD). The total acidity of the catalyst was obtained by integrating the area under the desorption curve.

TEM analysis was carried out to determine the size of Ni⁰, Pt⁰, and Pd⁰ particles on reduced samples. The experiments were carried out using an HRTEM 2010 JEOL LaB6 microscope (200 kV) (Tokyo, Japan). Data analysis was performed by using ImageJ software (Version 1.54). For this purpose, a minimum of 150 or 300 metallic particles were counted in each sample, depending on the metal source, transition or noble metal, respectively. The dispersion of metal-based catalysts, which is the ratio between the total number of metal atoms present on the surface of the catalyst and the total number of metal atoms, was determined assuming that Ni, Pt, and Pd are spherical particles, through the following equation:

$$D = 6/d \cdot p,$$

where d is the mean particle size and p is the atomic density.

4.4. Thermogravimetric Analysis Procedure

The samples used for the TGA experiments were prepared by compression molding technique. The HDPE and catalyst, both in powder form, were first mechanically mixed in a mass ratio of 9/1 and then heated in a hydraulic press at 140 °C and 3 tons of pressure for 5 min [64].

The thermogravimetric experiments were performed using a Setaram TGA 92-16.18 thermobalance (Austin, TX, USA) under a H₂ atmosphere, at a continuous flow rate of 30 mL/min. The temperature varied between 20 and 700 °C, at different heating rates (2, 5, 10, 15 °C/min). To avoid the presence of oxygen, a nitrogen purge of 15 min was performed before each experiment.

5. Conclusions

In this work, the kinetic parameters of the thermal and catalytic conversions of HDPE under a H₂ atmosphere were determined by non-isothermal TGA experiments, applying two different model-free methods, namely Flynn–Wall–Ozawa and Kissinger–Akahira–Sunose. The results show that the thermal degradation of HDPE at the lowest heating rate takes place in the range of 433–473 °C, which means that a high energy input is required.

Nevertheless, the addition of H-USY (15) and H-ZSM-5 (11.5) zeolites has a positive effect on the degradation process, allowing the temperature at which mass loss is 5% to be reduced by 162 and 115 °C, respectively.

The kinetic data for HDPE thermal degradation show that E_a values increase with conversion (from 211 to 234 kJ/mol) and that an average value of 227 kJ/mol is obtained regardless of the model-free method used (FWO or KAS).

In the presence of H-USY (15) and H-ZSM-5 (11.5) catalysts, E_a suffers a significant decrease and becomes highly dependent on conversion. However, the average E_a value obtained for the FWO and KAS methods is very similar. For H-USY (15), it ranges from 116 to 122 kJ/mol, while for H-ZSM-5, it is much lower and varies between 77 and 81 kJ/mol. The variation in E_a with the extent of reaction is an indication of the presence of a multi-step complex reaction mechanism.

The addition of a metal source to the H-USY (15) and H-ZSM-5 (11.5) zeolites also leads to a significant reduction in the apparent E_a of the reaction compared to the thermal process. Conversely, a slight increase in E_a is observed compared to the respective parent systems. This is probably related to the contribution of the dehydrogenation/hydrogenation reactions to the overall mechanism and thus, to the resulting E_a .

In conclusion, both parent and metal-based H-USY (15) and H-ZSM-5 (11.5) zeolites can greatly reduce the energy barrier and corresponding energy consumption for HDPE hydrocracking compared to thermal conditions, thus promoting a more sustainable conversion of plastic waste.

As a final point, it is also important to recall that HDC is a complex reaction, involving a multi-step mechanism. The elucidation of the mechanisms underlying complex processes is very challenging, and extensive kinetic studies and model simulations are needed to gain a deeper understanding. In this preliminary investigation on the kinetics of HDPE hydrocracking, a meaningful estimate of the average value for the apparent E_a associated with the multistep process of each of the thermal and catalytic systems studied was obtained. However, to gain deeper mechanistic insights into the HDC reaction, it would be beneficial to apply advanced iso-conversional methods (AIC), which use numerical integration over small temperature intervals as a component of E_a evaluation, in association with a model-free methodology to determine $\ln A$. Further studies are in progress to address this topic.

Supplementary Materials: The following supporting information can be downloaded at: <https://www.mdpi.com/article/10.3390/catal14080514/s1>, Figure S1: PXRD diffractograms of parent and metal-based (Ni, Pt, Pd) H-USY (15) (A) and identification of Ni0, Pt0 and Pd0 species on XRD diffractograms (B); Figure S2: PXRD diffractograms of parent and metal-based (Ni, Pt, Pd) H-ZSM-5 (11.5) (A) and identification of Ni0, Pt0 and Pd0 species on XRD diffractograms (B); Figure S3- TGA profiles at distinct β (5, 10, 15 and 20 °C/min) for Ni-, Pt-, and Pd-based HUSY (A,C,E) and H-ZSM-5 (B,D,F) zeolites. Figure S4: TEM images of Ni-, Pt-, and Pd-based H-USY (15) and H-ZSM-5 (11.5) zeolites. Table S1: Metallic properties of metal-based H-USY (15) and H-ZSM-5 zeolites (11.5).

Author Contributions: Conceptualization, C.S.C., M.R.R., J.M.S. and A.F.; methodology, C.S.C. and A.F.; validation, C.S.C., A.F. and M.M.; formal analysis, C.S.C.; investigation, C.S.C., A.F. and M.M.; writing—original draft preparation, C.S.C.; writing—review and editing, C.S.C., M.R.R. and J.M.S.; visualization, C.S.C.; supervision, M.R.R. and J.M.S.; project administration, M.R.R. and J.M.S.; funding acquisition, M.R.R. and J.M.S. All authors have read and agreed to the published version of the manuscript.

Funding: This research was funded by Fundação para a Ciência e Tecnologia (FCT) [Project UIDB/00100/2020 (DOI 10.54499/UIDB/00100/2020), Project UIDP/00100/2020 (DOI 10.54499/UIDP/00100/2020), Project LA/P/0056/2020 (DOI 10.54499/LA/P/0056/2020), and (ERANETMED/0003/201). Cátia S. Costa is grateful for the PhD fellowship of the FCT-CATSUS program (PD/BD/12862/2017). The work is also part of the TED2021-129688B project, funded by MCIN/AEI/10.13039/501100011033 and by the European Union "NextGenerationEU"/PRTR. The content of this publication does not reflect the official opinion of the European Union. Responsibility for the information and views expressed in this paper lies entirely with the authors.

Data Availability Statement: Data are contained within the article or Supplementary Material.

Conflicts of Interest: The authors declare no conflicts of interest.

References

1. Mrowiec, B. Plastics in the circular economy (CE). *Environ. Prot. Nat. Resour. J. Inst. Environ. Prot. Res. Inst.* **2018**, *29*, 16–19. [[CrossRef](#)]
2. Al-Salem, S.M.; Lettieri, P.; Baeyens, J. Recycling and recovery routes of plastic solid waste (PSW): A review. *Waste Manag.* **2009**, *29*, 2625–2643. [[CrossRef](#)] [[PubMed](#)]
3. Al-Salem, S.M.; Antelava, A.; Constantinou, A.; Manos, G.; Dutta, A. A review on thermal and catalytic pyrolysis of plastic solid waste (PSW). *J. Environ. Manag.* **2017**, *197*, 177–198. [[CrossRef](#)] [[PubMed](#)]
4. Mohanraj, C.; Senthilkumar, T.; Chandrasekar, M. A review on conversion techniques of liquid fuel from waste plastic materials. *Int. J. Energy Res.* **2017**, *41*, 1534–1552. [[CrossRef](#)]
5. Panda, A.K. Thermo-catalytic degradation of different plastics to drop in liquid fuel using calcium bentonite catalyst. *Int. J. Ind. Chem.* **2018**, *9*, 167–176. [[CrossRef](#)]
6. Ratnasari, D.K.; Nahil, M.A.; Williams, P.T. Catalytic pyrolysis of waste plastics using staged catalysis for production of gasoline range hydrocarbon oils. *J. Anal. Appl. Pyrolysis* **2017**, *124*, 631–637. [[CrossRef](#)]
7. Almeida, D.; de Fátima Marques, M. Thermal and Catalytic Pyrolysis of Polyethylene Plastic Waste. *Polimeros* **2015**, *26*, 1–8. [[CrossRef](#)]
8. Socci, J.; Osatiashtiani, A.; Kyriakou, G.; Bridgwater, T. The catalytic cracking of sterically challenging plastic feedstocks over high acid density Al-SBA-15 catalysts. *Appl. Catal. A Gen.* **2019**, *570*, 218–227. [[CrossRef](#)]
9. Khedri, S.; Elyasi, S. Kinetic analysis for thermal cracking of HDPE: A new isoconversional approach. *Polym. Degrad. Stab.* **2016**, *129*, 306–318. [[CrossRef](#)]
10. Kumar, S.; Singh, R.K. Pyrolysis kinetics of waste high-density polyethylene using thermogravimetric analysis. *Int. J. ChemTech Res.* **2014**, *6*, 131–137.
11. Kumar, A.; Mylapilli, S.V.P.; Reddy, S.N. Thermogravimetric and kinetic studies of metal (Ru/Fe) impregnated banana pseudostem (*Musa acuminata*). *Bioresour. Technol.* **2019**, *285*, 121318. [[CrossRef](#)] [[PubMed](#)]
12. Kayacan, İ.; Doğan, Ö.M. Pyrolysis of Low and High Density Polyethylene. Part I: Non-isothermal Pyrolysis Kinetics, Energy Sources, Part A Recover. *Util. Environ. Eff.* **2008**, *30*, 385–391. [[CrossRef](#)]
13. Encinar, J.M.; González, J.F. Pyrolysis of synthetic polymers and plastic wastes. Kinetic study. *Fuel Process. Technol.* **2008**, *89*, 678–686. [[CrossRef](#)]
14. Fernandes, G.J.T.; Fernandes, V.J.; Araujo, A.S. Catalytic degradation of polyethylene over SAPO-37 molecular sieve. *Catal. Today* **2002**, *75*, 233–238. [[CrossRef](#)]
15. Budrugaec, P. Theory and practice in the thermoanalytical kinetics of complex processes: Application for the isothermal and non-isothermal thermal degradation of HDPE. *Thermochim. Acta* **2010**, *500*, 30–37. [[CrossRef](#)]
16. Araújo, A.S.; Fernandes, V.J.; Araujo, S.A.; Ionashiro, M. Kinetic evaluation of the pyrolysis of high density polyethylene over H-ALMCM-41 material. *Stud. Surf. Sci. Catal.* **2002**, *141*, 473–478. [[CrossRef](#)]
17. Street, S.; Centre, E.T.; Street, S. Catalytic degradation of high density polyethylene: An evaluation of mesoporous and microporous catalysts using thermal analysis. *Thermochim. Acta* **1997**, *294*, 65–69.
18. Garforth, A.; Yeuh-Hui, L.I.N.; Sharratt, P.; Dwyer, J. Catalytic Polymer Degradation for Producing Hydrocarbons over Zeolites. *Stud. Surf. Sci. Catal.* **1999**, *121*, 197–202. [[CrossRef](#)]
19. Coelho, A.; Costa, L.; Marques, M.D.M.; Fonseca, I.; Lemos, M.A.; Lemos, F. Using simultaneous DSC/TG to analyze the kinetics of polyethylene degradation-catalytic cracking using HY and HZSM-5 zeolites. *React. Kinet. Mech. Catal.* **2010**, *99*, 5–15. [[CrossRef](#)]
20. Munir, D.; Abdullah; Piepenbreier, F.; Usman, M.R. Hydrocracking of a plastic mixture over various micro-mesoporous composite zeolites. *Powder Technol.* **2017**, *316*, 542–550. [[CrossRef](#)]
21. Munir, D.; Irfan, M.F.; Usman, M.R. Hydrocracking of virgin and waste plastics: A detailed review. *Renew. Sustain. Energy Rev.* **2018**, *90*, 490–515. [[CrossRef](#)]
22. Khawam, A.; Flanagan, D.R. Role of isoconversional methods in varying activation energies of solid-state kinetics: II. Nonisothermal kinetic studies. *Thermochim. Acta* **2005**, *436*, 101–112. [[CrossRef](#)]
23. Ashraf, A.; Sattar, H.; Munir, S. A comparative applicability study of model-fitting and model-free kinetic analysis approaches to non-isothermal pyrolysis of coal and agricultural residues. *Fuel* **2019**, *240*, 326–333. [[CrossRef](#)]
24. Murichan, N.; Chertongchai, P. Kinetic Analysis of Thermal Degradation of Polyolefin Mixtures. *Int. J. Chem. Eng. Appl.* **2014**, *5*, 169–175. [[CrossRef](#)]
25. Sánchez-Jiménez, P.E.; Pérez-Maqueda, L.A.; Perejón, A.; Criado, J.M. Clarifications regarding the use of model-fitting methods of kinetic analysis for determining the activation energy from a single non-isothermal curve. *Chem. Cent. J.* **2013**, *7*, 25. [[CrossRef](#)] [[PubMed](#)]
26. Janković, B.; Adnadević, B.; Jovanović, J. Application of model-fitting and model-free kinetics to the study of non-isothermal dehydration of equilibrium swollen poly (acrylic acid) hydrogel: Thermogravimetric analysis. *Thermochim. Acta* **2007**, *452*, 106–115. [[CrossRef](#)]

27. Ravari, F.; Noori, M.; Ehsani, M. Thermal Stability and Degradation Kinetic Studies of PVA/RGO Using the Model-fitting and Isoconversional (model-free) Methods. *Fibers Polym.* **2019**, *20*, 472–480. [[CrossRef](#)]
28. Vyazovkin, S.; Chrissa, K.; Laura, M.; Lorenzo, D.; Koga, N.; Pijolat, M.; Roduit, B.; Sbirrazzuoli, N.; Josep, J. Thermochemical Acta ICTAC Kinetics Committee recommendations for collecting experimental thermal analysis data for kinetic computations. *Thermochim. Acta* **2014**, *590*, 1–23. [[CrossRef](#)]
29. Yao, F.; Wu, Q.; Lei, Y.; Guo, W.; Xu, Y. Thermal decomposition kinetics of natural fibers: Activation energy with dynamic thermogravimetric analysis. *Polym. Degrad. Stab.* **2008**, *93*, 90–98. [[CrossRef](#)]
30. Siddiqui, M.N.; Antonakou, E.V.; Redhwi, H.H.; Achilias, D.S. Kinetic analysis of thermal and catalytic degradation of polymers found in waste electric and electronic equipment. *Thermochim. Acta* **2019**, *675*, 69–76. [[CrossRef](#)]
31. Friedman, H.L. Kinetics of thermal degradation of char-forming plastics from thermogravimetry. Application to a phenolic plastic. *J. Polym. Sci. Part C Polym. Symp.* **1964**, *6*, 183–195. [[CrossRef](#)]
32. Flynn, J.H.; Wall, L.A. General Treatment of the Thermogravimetry of Polymers. *J. Res. Natl. Bur. Standards-Phys. Chem.* **1996**, *70*, 344–346. [[CrossRef](#)] [[PubMed](#)]
33. Flynn, J.H. The “temperature integral”—Its use and abuse. *Thermochim. Acta* **1997**, *300*, 83–92. [[CrossRef](#)]
34. Ozawa, T. A New Method of Analyzing Thermogravimetric Data. *Bull. Chem. Soc. Jpn.* **1965**, *38*, 1881–1886. [[CrossRef](#)]
35. Kissinger, H.E. Variation of peak temperature with heating rate in differential thermal analysis. *J. Res. Natl. Bur. Stand.* **1956**, *57*, 217. [[CrossRef](#)]
36. Vyazovkin, S.; Burnham, A.K.; Criado, J.M.; Pérez-Maqueda, L.A.; Popescu, C.; Sbirrazzuoli, N. ICTAC Kinetics Committee recommendations for performing kinetic computations on thermal analysis data. *Thermochim. Acta* **2011**, *520*, 1–19. [[CrossRef](#)]
37. Kumar, S.A.P.; Nagarajan, R.; Prasad, K.M.; Anand, B.; Murugavelh, S. Thermogravimetric study and kinetics of banana peel pyrolysis: A comparison of “model-free” methods. *Biofuels* **2019**, *13*, 129–138. [[CrossRef](#)]
38. Doyle, C.D. Estimating isothermal life from thermogravimetric data. *J. Appl. Polym. Sci.* **1962**, *6*, 639–642. [[CrossRef](#)]
39. Murray, P.; White, J. Kinetics of the thermal dehydration of clay. Part IV. Interpretation of the differential thermal analysis of the clay minerals. *Trans. Br. Ceram. Soc.* **1955**, *54*, 204–238.
40. Wong, S.; Ngadi, N.; Abdullah, T.A.T.; Inuwa, I.M. Catalytic Cracking of LDPE Dissolved in Benzene Using Nickel-Impregnated Zeolites. *Ind. Eng. Chem. Res.* **2016**, *55*, 2543–2555. [[CrossRef](#)]
41. Hamidzadeh, M.; Ghassemzadeh, M.; Tarlani, A.; Sahebdelfar, S. The effect of hydrothermal impregnation of Ni, Co, and Cu on HZSM-5 in the nitrogen oxide removal. *Int. J. Environ. Sci. Technol.* **2018**, *15*, 93–104. [[CrossRef](#)]
42. Awala, H.; Gilson, J.P.; Retoux, R.; Boullay, P.; Goupil, J.M.; Valtchev, V.; Mintova, S. Template-free nanosized faujasite-type zeolites. *Nat. Mater.* **2015**, *14*, 447–451. [[CrossRef](#)]
43. Caldeira, V.P.S.; Santos, A.G.D.; Oliveira, D.S.; Lima, R.B.; Souza, L.D.; Pergher, S.B.C. Polyethylene catalytic cracking by thermogravimetric analysis: Effects of zeolitic properties and homogenization process. *J. Therm. Anal. Calorim.* **2017**, *130*, 1939–1951. [[CrossRef](#)]
44. Abbasa, A.S.; Saber, M.G. Kinetics of Thermal Pyrolysis of High-Density Polyethylene. *Iraqi J. Chem. Pet. Eng.* **2018**, *19*, 13–19. [[CrossRef](#)]
45. Zhao, D.; Wang, X.; Miller, J.B.; Huber, G.W. The Chemistry and Kinetics of Polyethylene Pyrolysis: A Process to Produce Fuels and Chemicals. *ChemSusChem* **2020**, *13*, 1764–1774. [[CrossRef](#)]
46. Anene, A.F.; Fredriksen, S.B.; Sætre, K.A.; Tokheim, L.A. Experimental study of thermal and catalytic pyrolysis of plastic waste components. *Sustainability* **2018**, *10*, 3979. [[CrossRef](#)]
47. Costa, C.S.; Ribeiro, M.R.; Silva, J.M. Hydrocracking of HDPE over H-USY and mesostructure acidic materials: Accessibility and acidity effects. In Proceedings of the 8th International Symposium on Energy from Biomass and Waste—Venice 2020, Venice, Italy, 16–19 November 2020.
48. Costa, C.S.; Thi, H.D.; Van Geem, K.M.; Ribeiro, M.R.; Silva, J.M. Assessment of acidity and the zeolite porous structure on hydrocracking of HDPE. *Sustain. Energy Fuels* **2022**, *6*, 3611–3625. [[CrossRef](#)]
49. Shahbeig, H.; Nosrati, M. Pyrolysis of municipal sewage sludge for bioenergy production: Thermo-kinetic studies, evolved gas analysis, and techno-socio-economic assessment. *Renew. Sustain. Energy Rev.* **2020**, *119*, 109567. [[CrossRef](#)]
50. Das, P.; Tiwari, P. Thermal degradation kinetics of plastics and model selection. *Thermochim. Acta* **2017**, *654*, 191–202. [[CrossRef](#)]
51. Al-Salem, S.M.; Sharma, B.K.; Khan, A.R.; Arnold, J.C.; Alston, S.M.; Chandrasekaran, S.R.; Al-Dhafeeri, A.T. Thermal degradation kinetics of virgin polypropylene (PP) and PP with starch blends exposed to natural weathering. *Ind. Eng. Chem. Res.* **2017**, *56*, 5210–5220. [[CrossRef](#)]
52. Mortezaeikia, V.; Tavakoli, O.; Khodaparasti, M.S. A review on kinetic study approach for pyrolysis of plastic wastes using thermogravimetric analysis. *J. Anal. Appl. Pyrolysis* **2021**, *160*, 105340. [[CrossRef](#)]
53. Dhaundiyal, A.; Singh, S.B.; Hanon, M.M.; Rawat, R. Determination of Kinetic Parameters for the Thermal Decomposition of Parthenium hysterophorus. *Environ. Clim. Technol.* **2018**, *22*, 5–21. [[CrossRef](#)]
54. Volli, V.; Purkait, M.K. Physico-chemical properties and thermal degradation studies of commercial oils in nitrogen atmosphere. *Fuel* **2014**, *117*, 1010–1019. [[CrossRef](#)]
55. Sinfrônio, F.S.M.; Santos, J.C.O.; Pereira, L.G.; Souza, A.G.; Conceição, M.M.; Fernandes, V.J.; Fonseca, V.M. Kinetic of thermal degradation of low-density and high-density polyethylene by non-isothermal thermogravimetry. *J. Therm. Anal. Calorim.* **2005**, *79*, 393–399. [[CrossRef](#)]

56. Peterson, J.D.; Vyazovkin, S.; Wight, C.A. Kinetics of the thermal and thermo-oxidative degradation of polystyrene, polyethylene and poly(propylene). *Macromol. Chem. Phys.* **2001**, *202*, 775–784. [[CrossRef](#)]
57. Vyazovkin, S.; Sbirrazzuoli, N. Isoconversional kinetic analysis of thermally stimulated processes in polymers. *Macromol. Rapid Commun.* **2006**, *27*, 1515–1532. [[CrossRef](#)]
58. Singh, B.; Sharma, N. Mechanistic implications of plastic degradation. *Polym. Degrad. Stab.* **2008**, *93*, 561–584. [[CrossRef](#)]
59. Lin, Y.H.; Hwu, W.H.; Ger, M.D.; Yeh, T.F.; Dwyer, J. A combined kinetic and mechanistic modelling of the catalytic degradation of polymers. *J. Mol. Catal. A Chem.* **2001**, *171*, 143–151. [[CrossRef](#)]
60. Weitkamp, J. Catalytic Hydrocracking-Mechanisms and Versatility of the Process. *ChemCatChem* **2012**, *4*, 292–306. [[CrossRef](#)]
61. Tao, M.; Meng, X.; Xin, Z.; Bian, Z.; Lv, Y.; Gu, J. General Synthesis and characterization of well dispersed nickel-incorporated SBA-15 and its high activity in syngas methanation reaction. *Appl. Catal. A Gen.* **2016**, *516*, 127–134. [[CrossRef](#)]
62. Ramdoss, P.K.; Tarrer, A.R. High-temperature liquefaction of waste plastics. *Fuel* **1998**, *77*, 293–299. [[CrossRef](#)]
63. Miskolczi, N.; Juzsakova, T. Preparation and application of metal loaded ZSM-5 and γ -zeolite catalysts for thermo-catalytic pyrolysis of real end of life vehicle plastics waste. *J. Energy Inst.* **2019**, *92*, 118–127. [[CrossRef](#)]
64. Costa, C.S.; Muñoz, M.; Ribeiro, M.R.; Silva, J.M. A thermogravimetric study of HDPE conversion under a reductive atmosphere. *Catal. Today* **2020**, *379*, 192–204. [[CrossRef](#)]

Disclaimer/Publisher's Note: The statements, opinions and data contained in all publications are solely those of the individual author(s) and contributor(s) and not of MDPI and/or the editor(s). MDPI and/or the editor(s) disclaim responsibility for any injury to people or property resulting from any ideas, methods, instructions or products referred to in the content.